zebrafish
第73回日本血液学会学術集会総会, 名古屋, 2011年10月16日
口頭発表

7. Tomoko Inoue, Kasem Kulkeaw, Yuka Horio, Satoko Okayama, Chiyo Mizuochi, Koichi Akashi, Kenzaburo Tani, Daisuke Sugiyama
Variation in Hematopoietic Potential of Adult and Embryonic Skin-Derived iPSC Lines
第17回 日本遺伝子治療学会, 福岡, 2011年7月, 口頭発表 (英語)

8. 杉山大介, Kulkeaw Kasm, 水落ちよ, 堀尾有可, 井上朋子, 岡山聡子, Kanitta Srinoun
Fetal liver hematopoiesis and implications for haematotherapy
日本顕微鏡学会第67回学術講演会, 福岡, 2011年5月16日
口頭発表 (招聘指定講演)

9. 水落ちよ, Kulkeaw Kasm, 堀尾有可, 井上朋子, 岡山聡子, Kanitta Srinoun, 杉山大介
Regulation of HSCs in the mouse placental niche through SCF/c-Kit signaling
日本顕微鏡学会第67回学術講演会, 福岡, 2011年5月16日
口頭発表

10. 井上朋子, Kulkeaw Kasm, 堀尾有可, 水落ちよ, 岡山聡子, Kanitta Srinoun, 谷憲三朗, 杉山大介
Variation in hematopoietic potential of adult skin-derived iPSC lines.
日本顕微鏡学会第67回学術講演会, 福岡, 2011年5月16日
口頭発表

11. 杉山 大介, Kulkeaw Kasem, 水落 ちよ, 堀尾 有可, 井上 朋子, 岡山 聡子, Srinoun Kanitta
Fetal liver hematopoiesis and implications for haematotherapy
日本顕微鏡学会第67回学術講演会, 福岡, 2011年5月16日

12. 水落 ちよ, Kulkeaw Kasem, 堀尾 有可, 井上 朋子, 岡山 聡子, Srinoun Kanittal, 杉山 大介
Regulation of HSCs in the mouse placental niche through SCF/c-Kit signaling
日本顕微鏡学会第67回学術講演会, 福岡, 2011年5月16日

13. 井上 朋子, Kulkeaw Kasem, 堀尾 有可, 水落 ちよ, 岡山 聡子, Srinoun Kanitta, 谷 憲三朗, 杉山 大介

Variation in hematopoietic potential of adult skin derived iPSC lines

日本顕微鏡学会第 67 回学術講演会, 福岡, 2011 年 5 月 16 日

口頭発表

14. 岡山 聡子, Kulkeaw Kasem, 水落 ちよ, 堀尾 有可, 井上 朋子, 杉山 大介

Hepatoblasts comprise a niche for fetal liver erythropoiesis through cytokines

日本顕微鏡学会第 67 回学術講演会, 福岡, 2011 年 5 月 16 日

15. Srinoun Kanitta, 井上 朋子, Kulkeaw Kasem, Batchuluun Battsetseg, 水落 ちよ, 堀尾 有可, 岡山 聡子, Svasti Saovaros, Fucharon Suthat, 杉山 大介

Ninjin Yoeito and Juzen Taihoto Kampos accelerate mouse erythropoiesis in vitro

日本顕微鏡学会第 67 回学術講演会, 福岡, 2011 年 5 月 16 日

H．知的財産権の出願・登録状況

（予定を含む。）

1．特許取得

・ 発明の名称:　アセチル化酵素競合阻害因子Gm16515の新規用途

・ 代表発明者　　杉山　大介　　准教授　（　医学研究院　）

・ 出願番号:　特願2012-080211

・ 出願日:2012/3/30

・ 特許事務所:　三枝国際特許事務所

・ 担当者　　三角　可恵（　知的財産本部　）

2．実用新案登録

特になし

3.その他

特になし

別紙４

研究成果の刊行に関する一覧表

書籍

著者氏名	論文タイトル名	書籍全体の編集者名	書　籍　名	出版社名	出版地	出版年	ページ
Sugiyama D, Inoue T and Kulkeaw K.	Stem cell maintenance in embryos and adults.	Roger Kasunic	Year Book of SCIENCE & TECHNOLOGY 2011	McGRAW-HILL	New York	2011	258-261

雑誌

発表者氏名	論文タイトル名	発表誌名	巻号	ページ	出版年
Mizuochi M, Fraser ST, Biasch K, Horio Y, Kikushige Y, Tani K, Akashi K, Tavian M and Sugiyama D.	Intra-aortic clusters undergo endothelial to hematopoietic phenotypic transition during early embryogenesis.	PlosOne			In press
Inoue T, Tani K and Sugiyama D.	Mesodermal and Hematopoietic Differentiation from ES and iPS Cells.	Stem Cell Reviews and Reports			In press
Kulkeaw K, Inoue T, Mizuochi C, Horio Y, Ishihama Y and Sugiyama D.	Ectopic expression of Hmgn2 antagonizes mouse erythroid differentiation in vitro.	Cell Biol Int	36(2)	195-202	2012
Inoue T, Kulkeaw K, Okayama S, Tani K and Sugiyama D.	Variation in Mesodermal and Hematopoietic Potential of Adult Skin-derived Induced Pluripotent Stem Cell Lines in Mice.	Stem Cell Reviews and Reports	7(4)	958-968	2011
Sugiyama D, Kulkeaw K, Mizuochi C, Horio Y and Okayama S.	Hepatoblasts comprise a niche for fetal liver erythropoiesis through cytokine production	Biochem Biophys Res Commun.	410(2)	301-306	2011
Kulkeaw K, Ishitani T, Kanemaru T, Ivanovski O, Nakagawa M, Mizuochi C, Horio Y, Sugiyama D.	Cold exposure down-regulates zebrafish pigmentation.	Genes to Cells	16(4)	358-367	2011

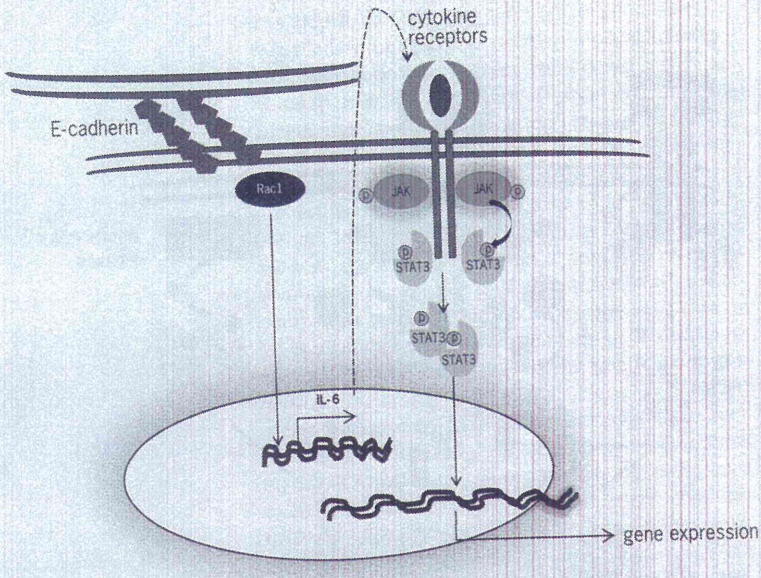

Fig. 2. Model of STAT3 activation by cadherin and Rac1/Cdc42. In an alternative mode of activation, cell–cell contact through cadherin engagement increases Rac1 and Cdc42 proteins, which induce IL-6 transcription. An increase in IL-6 production stimulates cytokine receptors, which then activate STAT3 through receptor-mediated activation.

of a Crohn's disease–like colitis, whereas immunohistochemical studies showed activated STAT3 expression in the intestines of patients with inflammatory bowel disease. Genome-wide association studies (GWAS) uncovered the single-nucleotide polymorphism, rs12948909, within the *STAT3* gene in patients with Crohn's disease and ulcerative colitis.

Role of STAT3 in cancer. STAT3 is constitutively activated in cancers of the breast, prostate, lung, head, and neck, as well as in multiple myeloma and leukemia. A constitutively active form of STAT3 alone is sufficient to transform cultured fibroblasts to anchorage independence (the ability of cells to proliferate in the absence of adhesion to extracellular matrix proteins) and points to a causal role for STAT3 in cancer development. Most of the described oncogenic functions of STAT3 depend on its Tyr^{705} phosphorylation status; however, an additional oncogenic role for STAT3 has been recently described that is dependent on serine phosphorylation and takes place in mitochondria. Recent evidence also suggests a crucial role for STAT3 in selectively inducing and maintaining a procarcinogenic inflammatory microenvironment, both at the initiation of malignant transformation and during cancer progression. STAT3 is linked to inflammation-associated tumorigenesis that is initiated by genetic alterations in malignant cells, as well as by many environmental factors, including chemical carcinogens, sunlight, infection, cigarette smoking, and stress.

Drug targets for STAT3 inhibition. The large body of data validating STAT3 as a target for cancer therapy, and the tolerance of normal cells for the loss of STAT3 function, has driven the effort to identify molecules that inhibit STAT3. In cell lines, inhibition of STAT3 activity using genetic or pharmacologic approaches reduces cancer cell growth and induces apoptosis. A few of the strategies to inhibit STAT3 that are currently under exploration are based on targeting the different structural domains of the protein and indirect targeting of the upstream components of the pathway, including the inhibition of tyrosine kinases that block aberrant STAT3 signaling. As STAT3 is negatively regulated through numerous mechanisms [for example, suppressors of cytokine signaling (SOCS), protein inhibitor of activated STAT (PIAS), protein phosphatases, and ubiquitin-dependent proteasomal degradation], additional strategies targeting STAT3 are also being actively investigated. Although few clinical trials targeting STAT3 are in place in 2011, it is likely to become an important targeting tool in the future as more is understood about the significance of this molecule in cancer and other diseases.

For background information *see* CANCER (MEDICINE); CELL (BIOLOGY); CELL BIOLOGY; CELLULAR IMMUNOLOGY; CYTOKINE; GENE; ONCOGENES; ONCOLOGY; PROTEIN; PROTEIN KINASE; SIGNAL TRANSDUCTION; TRANSCRIPTION; TUMOR SUPPRESSOR GENES in the McGraw-Hill Encyclopedia of Science & Technology.

Rachel A. Altura

Bibliography. B. B. Aggarwal et al., Signal transducer and activator of transcription-3, inflammation, and cancer: How intimate is the relationship?, *Ann. N. Y. Acad. Sci.*, 1171:59–76, 2009; S. M. Holland et al., STAT3 mutations in the hyper-IgE syndrome, *N. Engl. J. Med.*, 357:1608–1619, 2007; G. Niu et al., Role of Stat3 in regulating p53 expression and function, *Mol. Cell. Biol.*, 25(17):7432–7440, 2005; H. Yu, D. Pardoll, and R. Jove, STATs in cancer inflammation and immunity: A leading role for STAT3, *Nat. Rev. Cancer*, 9:798–809, 2009; P. Yue and J. Turkson, Targeting STAT3 in cancer: How successful are we?, *Expert Opin. Investig. Drugs*, 18(1):45–56, 2009.

Stem cell maintenance in embryos and adults

Stem cells are capable of self-renewal. Provided they have the ability to differentiate into various types of mature cells, they are classified as pluripotent stem cells. Examples of well-studied stem cell types include embryonic stem cells, induced pluripotent stem cells, and tissue-specific stem cells, which enable the corresponding tissues to sustain cell-based homeostasis and which contribute to regenerative mechanisms. These tissue-specific stem cells have been found in blood, nervous tissue, mesenchyme, and skin, and they are regulated both intrinsically and extrinsically. Intrinsic regulation is programmed by genes and transcription factors that are active in the stem cells themselves, whereas extrinsic regulation is accomplished by cytokines and matrices secreted by niche cells surrounding stem cells. Among tissue-specific stem cells, hematopoietic stem cells (HSCs) are the stem cells in the blood lineage and

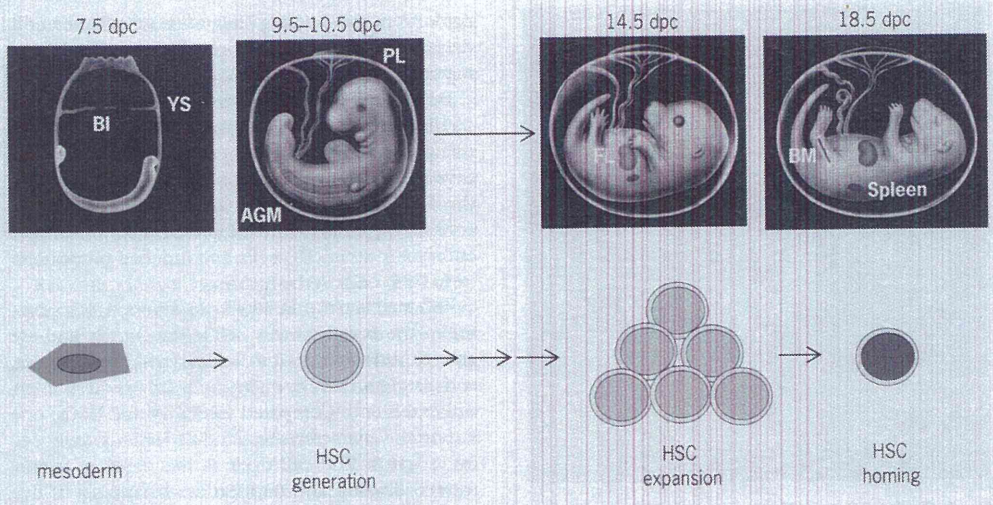

Fig. 1. Schema of hematopoietic development during embryogenesis in mice. Hematopoietic stem cells (HSCs) are generated in the yolk sac (YS), aorta-gonad-mesonephros (AGM) region, and placenta (PL) from early- to mid-gestation periods [7.0–11.0 days postcoitum (dpc)]. They expand to the fetal liver (FL) at midgestation and later migrate (home) temporarily to the fetal spleen and finally to fetal bone marrow (BM). The blood island (BI) is the first site of hematopoiesis.

they have been used in patients for transplantation therapy in the fields of hematology and regenerative medicine. Most sources of HSCs rely on healthy donors and umbilical cord blood. However, problems remain in HSC transplantation, including shortages of donors and risks for donors [for example, transplant rejection and graft-versus-host disease (GVHD)]. Understanding of HSC regulation, especially with regard to niche cells, will enable us to improve HSC therapy through novel stem cell engineering.

HSC maintenance in embryos. In the mouse embryo, the site for blood production changes during the 20-day gestation period. HSCs are initially generated in the yolk sac, aorta-gonad-mesonephros region, and placenta. This initial stage is followed by expansion of HSCs into the fetal liver. Then, later in gestation, after residing temporarily in the fetal spleen, HSCs finally reside in the fetal bone marrow (**Fig. 1**).

The yolk sac is a membranous sac attaching to an embryo and contains the blood islands, which are the first site of hematopoiesis (the process by which the cellular elements of the blood are formed), particularly erythropoiesis (the process by which erythrocytes are formed), and development of the circulatory system after 7.0 days postcoitum (dpc, which is a designation of embryonic age). Among the three germ layers (endoderm, mesoderm, and ectoderm), mesodermal cells differentiate into both hematopoietic cells inside and endothelial cells (ECs) outside of the blood islands. Endodermal cells differentiate into unclassified mesenchymal cells (MCs) that fill out the other spaces of the yolk sac. Therefore, both ECs and MCs likely comprise a niche for yolk sac hematopoiesis. Members of the Hedgehog family of proteins, which are important regulators of many developmental processes, reportedly function in yolk sac hematopoiesis, but the niche regulation of yolk sac hematopoiesis remains unclear.

After yolk sac hematopoiesis, HSCs are generated in the aorta-gonad-mesonephros region, where aggregates of the cells expressing HSC surface protein markers (for example, c-Kit, CD31, and CD34) are observed and display HSC activity. These aggregates are named hematopoietic clusters or aortic clusters. At 10.5 dpc, these hematopoietic clusters are frequently observed attaching to the walls of large arteries (as if they are generated from EC layers). Because the aorta-gonad-mesonephros region consists of ECs, gonad cells, mesonephros cells, and unclassified MCs, the cells likely comprise a niche for HSC generation. MCs of the aorta-gonad-mesonephros region reportedly increase the number of HSCs at 10.5 dpc through the Hedgehog signaling pathway. In addition, ECs of the aorta-gonad-mesonephros region at 10.5 dpc likely have a role in HSC regulation through secretion of a cytokine known as stem cell factor (SCF). Taken together, several cell components comprise a niche for HSC generation.

The placenta connects the fetus to the mother and is highly vascularized in structure. It functions not only in gas exchange and fetal nutrition but also in hematopoiesis at 8.5–13.5 dpc. In particular, HSCs are generated in the placenta at 11.5 dpc, with their numbers dramatically increasing at 11.5–12.5 dpc. Similar to the aorta-gonad-mesonephros region, hematopoietic clusters are observed in the vasculature of the placenta (**Fig. 2**). To examine the roles of niche cells surrounding the clusters, they were isolated by both laser-capture microdissection and flow cytometry methods. Among several cytokine genes, only the *SCF* gene was expressed particularly in the niche cells. Administration of blocking antibody to c-Kit, the receptor for SCF, clearly demonstrated that SCF/c-Kit signaling is pivotal in HSC regulation in the placenta.

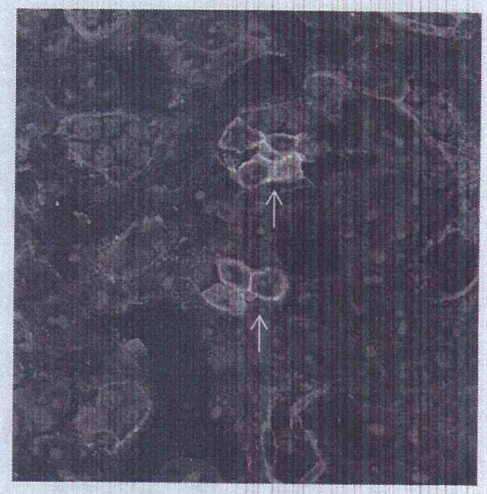

Fig. 2. Confocal image of hematopoietic clusters in the aorta of the placenta (PL) at 11.5 days postcoitum (dpc). Sections of the placenta were made from ICR mouse strain embryos at 11.5 dpc, stained with antibodies (CD34 and c-Kit). CD34/c-Kit double-positive cells indicate hematopoietic clusters (arrows), equivalent to hematopoietic stem cells (HSCs). TOTO-3 was used as a stain for nuclei.

After HSCs are generated in the yolk sac, aorta-gonad-mesonephros region, and placenta, they migrate to the fetal liver, where the numbers of HSCs dramatically increase at 12–16 dpc and they differentiate particularly into erythrocytes. The fetal liver consists of hepatoblasts (hepatocyte precursors), ECs, and hematopoietic cells (as well as other cells). Among them, hepatoblasts have a role in HSC differentiation, particularly erythropoiesis through secretion of mainly erythropoietin (EPO), a cytokine that regulates erythropoiesis, and SCF. In addition, hepatoblasts increase the number of HSCs through production of several other cytokines, including angiopoietin-like 3 (Angptl3), insulin-like growth factor-2 (IGF2), SCF, and thrombopoietin (TPO). Taken together, hepatoblasts comprise a niche for HSC regulation through cytokine secretion. However, it remains unclear how HSCs maintain their self-renewal capability under extensive cytokine exposures that stimulate HSC differentiation. Further investigation is necessary to resolve how niche cells regulate HSC potency in the fetal liver.

After the numbers of HSCs increase in the fetal liver, they migrate to the fetal spleen. At this location, HSCs differentiate particularly into macrophages at 13.5–14.5 dpc. Fetal spleen-derived stromal cells enable HSCs to differentiate into macrophages, but not lymphocytes. It is not known how HSC differentiation is regulated in this tissue. After transient hematopoiesis in the fetal spleen, HSCs gradually migrate to the bone marrow after 16.5 dpc, and they remain there for the duration of their lives. Here, the stromal cells and MCs secrete a chemokine, called CXC-chemokine ligand 12 (CXCL12), which attracts the HSCs expressing the CXCL12 receptor CXCR-4 and results in HSCs migrating to the bone marrow. Aside from this homing (migration) mechanism, little is known about niche regulation in fetal bone marrow.

During embryogenesis, spatiotemporal regulation of HSCs occurs extrinsically by several niche cell components. Accumulation of evidence about embryonic HSC regulation by niche cells will facilitate the development of novel therapies of in vitro generation, expansion, and differentiation of HSCs from embryonic stem (ES) cells and induced pluripotent stem (iPS) cells in the future.

HSC maintenance in adults. In adults, HSCs residing in the bone marrow self-renew slowly and are able to differentiate into leukocytes, erythrocytes, and platelets, thereby maintaining homeostasis in peripheral blood. Compared to embryonic HSCs, one important characteristic of adult HSCs is their cell cycle status. The cell cycle is the series of events for cell division and duplication. It consists of five phases: G0, G1, S, G2, and M phases. The G0 phase is the state in which cells stop cell division and is called quiescence. The cell cycle status of most adult HSCs is G0 phase, whereas that of embryonic HSCs is a non-G0 phase. This quiescent status is essential in interrupting the exhaustion of HSCs and is tightly regulated by surrounding niche cells. In response to blood cell loss, HSCs exit from quiescence, divide, and differentiate into mature blood cells.

Bone marrow consists of several kinds of cells, including osteoblasts (which generate bone), ECs, neural cells, fibroblasts (stellate connective tissue cells found in fibrous tissue), hematopoietic cells, and MCs. Several reports suggest that both osteoblasts and ECs comprise niches for HSC regulation. Osteoblastic niches are located at the endosteal region (the inner surface of bone), where HSCs bind through their expression of adhesion molecules, including neural cadherin (N-cadherin) and very late antigen 4 (VLA4) integrin, which bind to the same and/or other adhesion molecules expressed on osteoblasts. Moreover, N-cadherin interacts with the extracellular matrix, including an acidic glycoprotein (osteopoietin) and a hyaluronic acid secreted from osteoblasts. These adhesion molecules are important for retaining HSCs in the osteoblastic niches. To maintain their quiescent status in the osteoblastic niches, osteoblasts secrete several molecules: (1) vascular endothelial growth factor (angiopoietin-1), (2) TPO, (3) SCF, and (4) CXCL12. Angiopoietin-1, TPO, SCF, and CXCL12 respectively bind to their corresponding receptors of Tie2, MPL, c-Kit, and CXCR4 expressed on HSCs. The bindings of these molecules result in inhibition of HSC division to maintain the quiescent status of HSCs.

In contrast to the osteoblastic niches, HSCs residing in endothelial niches are not quiescent. The endothelial niches are located in the center of the bone marrow cavity and are composed of sinusoid ECs expressing vascular endothelial cadherin (VE-cadherin). In response to blood cell loss, sinusoid ECs secrete CXCL12 to attract HSCs from osteoblastic niches to endothelial niches, resulting in HSC proliferation and differentiation to replenish blood cells.

The endothelial niches are also important for regulating HSC migration from the osteoblastic niches to blood circulation. Administration of granulocyte colony-stimulating factor (G-CSF) causes endothelial niches to secrete neutrophil protease, which degrades adhesion molecules and keeps HSCs in the osteoblastic niches. Using this mechanism, HSCs are harvested from peripheral blood by G-CSF administration and are clinically used for HSC transplantation therapy.

Recently, it has been reported that mesenchymal stem cells (MSCs) expressing nestin, an intermediate filament protein, constitute an essential niche in the bone marrow. Loss of nestin-expressing MSCs reduces the number and homing capacity of HSCs. However, it remains unclear how MSCs cooperate with osteoblastic and endothelial niches.

The quiescent status of HSCs is regulated extrinsically by several niche cell components. With this in mind, stem cells in leukemia are considered to be an important target for therapy because leukemic stem cells may be quiescent in osteoblastic niches, causing relapse of leukemia after complete remission. Thus, understanding of adult HSC regulation by niche cells will facilitate the development of novel technologies to freely control the quiescent status of HSCs and leukemic stem cells, ultimately leading to therapies targeting leukemic stem cells as well as HSC expansion and differentiation in the future.

For background information *see* CELL (BIOLOGY); CELL CYCLE; CELL DIFFERENTIATION; CELL LINEAGE; CYTOKINE; EMBRYOLOGY; EMBRYONIC DIFFERENTIATION; GENETIC ENGINEERING; HEMATOPOIESIS; REGENERATIVE BIOLOGY; STEM CELLS; TRANSPLANTATION BIOLOGY in the McGraw-Hill Encyclopedia of Science & Technology.

Daisuke Sugiyama; Tomoko Inoue; Kasem Kulkeaw

Bibliography. M. J. Kiel and S. Morrison, Uncertainty in the niches that maintain haematopoietic stem cells, *Nat. Rev. Immunol.*, 8:290–300, 2008; Z. Li and L. Li, Understanding hematopoietic stem-cell microenvironments, *Trends Biochem. Sci.*, 31:589–595, 2006; S. Méndez-Ferrer et al., Mesenchymal and haematopoietic stem cells form a unique bone marrow niche, *Nature*, 466:829–834, 2010; H. K. Mikkola et al., Placenta as a site for hematopoietic stem cell development, *Exp. Hematol.*, 33:1048–1054, 2005; T. Sasaki et al., Regulation of hematopoietic cell clusters in the placental niche through SCF/Kit signaling in embryonic mouse, *Development*, 137:3941–3952, 2010; D. Sugiyama and K. Tsuji, Definitive hematopoiesis from endothelial cells in the mouse embryo; a simple guide, *Trends Cardiovasc. Med.*, 16:45–49, 2006; D. Sugiyama et al., Hepatoblasts comprise a niche for fetal liver erythropoiesis through cytokine production, *Biochem. Biophys. Res. Commun.*, 410:301–306, 2011; A. Trumpp, M. Essers, and A. Wilson, Awakening dormant haematopoietic stem cells, *Nat. Rev. Immunol.*, 10:201–209, 2010; A. Wilson and A. Trumpp, Bone-marrow haematopoietic-stem-cell niches, *Nat. Rev. Immunol.*, 6:93–106, 2006.

Strategic decision making

Strategic decisions are decisions that critically influence the performance and survival of a firm. These strategic decisions are typically made by the senior managers of a firm, and generally involve high levels of uncertainty and complexity, occur in dynamic contexts, and include many different stakeholders, often with conflicting interests. Examples of strategic decisions include deciding whether a firm should collaborate with another firm to develop an innovative new product or go it alone, and whether a company should diversify into a new industry or market as opposed to concentrating on its core businesses.

A common theme—risk—underlies many of the theories and perspectives used to examine strategic decision making. Consistent with common usage, managers use the term risk to refer to the possibility of outcomes that are worse than their expected levels, and the degree to which this poor performance could hurt managers and their firms. This usage of risk differs from the usage in many academic fields that associate risk with variability of outcomes or choices involving well-specified potential outcomes, where each outcome is associated with a probability of occurrence. Researchers of strategic decision making generally use the term risk when referring to decisions that involve uncertainty or ambiguity.

Three theoretical perspectives, namely, the behavioral theory of the firm (BTOF), behavioral decision theory (BDT), and agency theory, dominate the work on strategic decision making. These theories are described in the following text.

Behavioral theory of the firm (BTOF). According to this theory, firms consist of coalitions of stakeholders. As such (and in contrast to traditional economic conceptualizations of firms as entities with a single goal or a well-defined set of many goals), firms have aspiration levels on many dimensions of performance. That is, firms seek to achieve desired levels of performance related to areas such as sales, profits, and so on. Various factors influence aspiration, including a firm's performance relative to its peers and the firm's historical performance. The theory predicts that the firm will make few changes to its existing routines and will operate as usual when the performance of a firm exceeds its aspiration level. However, when the performance of a firm falls below its aspiration level, the firm will seek to raise its performance by making changes that typically increase firm risk (see **illustration**). In this theory (and again in contrast to traditional economic theory), firms do not seek optimal results; rather, they seek to "satisfice," or produce good-enough results; in this context, the term satisfice refers to aiming to achieve satisfactory results. Empirical work on the behavioral theory of the firm has used field or archival data on firms.

Although the above description captures the essence of the theory, it should be noted that the theory also takes into account contingent factors that influence the likelihood that firms will change their routines in response to performance below

OPEN ACCESS Freely available online

PLoS one

Intra-Aortic Clusters Undergo Endothelial to Hematopoietic Phenotypic Transition during Early Embryogenesis

Chiyo Mizuochi[1], Stuart T. Fraser[2], Katia Biasch[3], Yuka Horio[1], Yoshikane Kikushige[4], Kenzaburo Tani[5], Koichi Akashi[4], Manuela Tavian[3], Daisuke Sugiyama[1]*

1 Department of Hematopoietic Stem Cells,SSP Stem Cell Unit, Kyushu University Faculty of Medical Sciences, Fukuoka, Japan, **2** Laboratory of Blood Cell Development, Disciplines of Physiology, Anatomy and Histology, School of Medical Sciences, University of Sydney, Camperdown, New South Wales, Australia, **3** Unité 682 INSERM, Strasbourg, France, **4** Department of Medicine and Biosystemic Science, Kyushu University Graduate School of Medical Sciences, Fukuoka, Japan, **5** Department of Molecular Genetics, Medical Institute of Bioregulation, Kyushu University, Fukuoka, Japan

Abstract

Intra-aortic clusters (IACs) attach to floor of large arteries and are considered to have recently acquired hematopoietic stem cell (HSC)-potential in vertebrate early mid-gestation embryos. The formation and function of IACs is poorly understood. To address this issue, IACs were characterized by immunohistochemistry and flow cytometry in mouse embryos. Immunohistochemical analysis revealed that IACs simultaneously express the surface antigens CD31, CD34 and c-Kit. As embryos developed from 9.5 to 10.5 dpc, IACs up-regulate the hematopoietic markers CD41 and CD45 while down-regulating the endothelial surface antigen VE-cadherin/CD144, suggesting that IACs lose endothelial phenotype after 9.5 dpc. Analysis of the hematopoietic potential of IACs revealed a significant change in macrophage CFC activity from 9.5 to 10.5 dpc. To further characterize IACs, we isolated IACs based on CD45 expression. Correspondingly, the expression of hematopoietic transcription factors in the CD45(neg) fraction of IACs was significantly up-regulated. These results suggest that the transition from endothelial to hematopoietic phenotype of IACs occurs after 9.5 dpc.

Citation: Mizuochi C, Fraser ST, Biasch K, Horio Y, Kikushige Y, et al. (2012) Intra-Aortic Clusters Undergo Endothelial to Hematopoietic Phenotypic Transition during Early Embryogenesis. PLoS ONE 7(4): e35763. doi:10.1371/journal.pone.0035763

Editor: Alfons Navarro, University of Barcelona, Spain

Received March 3, 2011; **Accepted** March 22, 2012; **Published** April 27, 2012

Funding: This research was supported in part by the Project for Realization of Regenerative Medicine, Special Coordination Funds for Promoting Science and Technology of the Ministry of Education, Science, Sports and Culture (www.mext.go.jp/english); and SAKURA program of the Japan Society for the Promotion of Science (www.jsps.go.jp/english/index.html). The funders had no role in study design, data collection and analysis, decision to publish, or preparation of the manuscript.

Competing Interests: The authors have declared that no competing interests exist.

* E-mail: ds-mons@yb3.so-net.ne.jp

Introduction

During mouse embryogenesis, hematopoiesis begins at the extra-embryonic yolk sac (YS) at 7.5 days post-coitum (dpc) and shifts to fetal liver after mid-gestation, then to spleen and finally to bone marrow shortly before birth. There are two distinct waves of hematopoietic emergence: a transient wave, primarily restricted to erythropoiesis in YS blood islands prior to the connection of the circulation from the YS to the embryo; and a definitive wave originating in both the YS and embryo proper. The embryonic site has been identified in the aortic region, in the para-aortic splanchnopleura (p-Sp)/aorta-gonad-mesonephros (AGM) region [1–6]. Functional hematopoietic stem cells (HSCs) that can reconstitute adult recipients are first identified in the AGM region at 10.5 dpc after ex vivo organ culture [7]. The cells at 10.5 dpc that were not cultured ex vivo rarely reconstitute adult recipients, whereas those at 11.5 dpc can regardless [7–9]. Therefore, the cells that acquire HSC activity after culture step, have been termed "pre-HSC"s. Although several reports characterize the surface marker expression on both pre-HSCs at 10.5 dpc and HSCs at 11.5 dpc, the developmental process of HSC generation still remains unclear [8–11]. Cell populations capable of reconstituting neonatal recipients are detected in the p-Sp/AGM region at 9.5 dpc [12–13]. These observations suggest that ancestor cells of HSC from the p-Sp/AGM region at 9.5 dpc require special microenvironments to acquire HSC activity and that HSCs undergo phenotypic changes from 9.5 to 10.5 dpc. In the AGM region, intra-aortic/arterial clusters (IACs) are observed attached to floors of large arteries in several species including chicken, mouse and humans [3]. Mouse IACs have been characterized morphologically and are primarily located in three large arteries, namely, the dorsal aorta (DA), the omphalomesenteric (vitelline) artery (OMA; VA) and the umbilical artery (UA) [3,14–15]. IACs express both hematopoietic (CD41 and CD45) and endothelial (CD31, CD34 and VE-cadherin) surface markers [3,15–16] suggesting that IACs are likely equivalent to ancestor cells of HSC and/or pre-HSCs and are derived from endothelial cells (ECs) at aortic/arterial regions. Although recent genetic approaches and novel tracing methods demonstrate that IACs are derived from ECs in zebrafish and mice, it is unclear how IACs form and acquire HSC activity [17–25].

To address how IACs form and function in HSC generation, we first visualized IACs by immunohistochemistry and confocal imaging and were found to simultaneously express CD31, CD34 and c-Kit. This approach enabled us to investigate the phenotypic

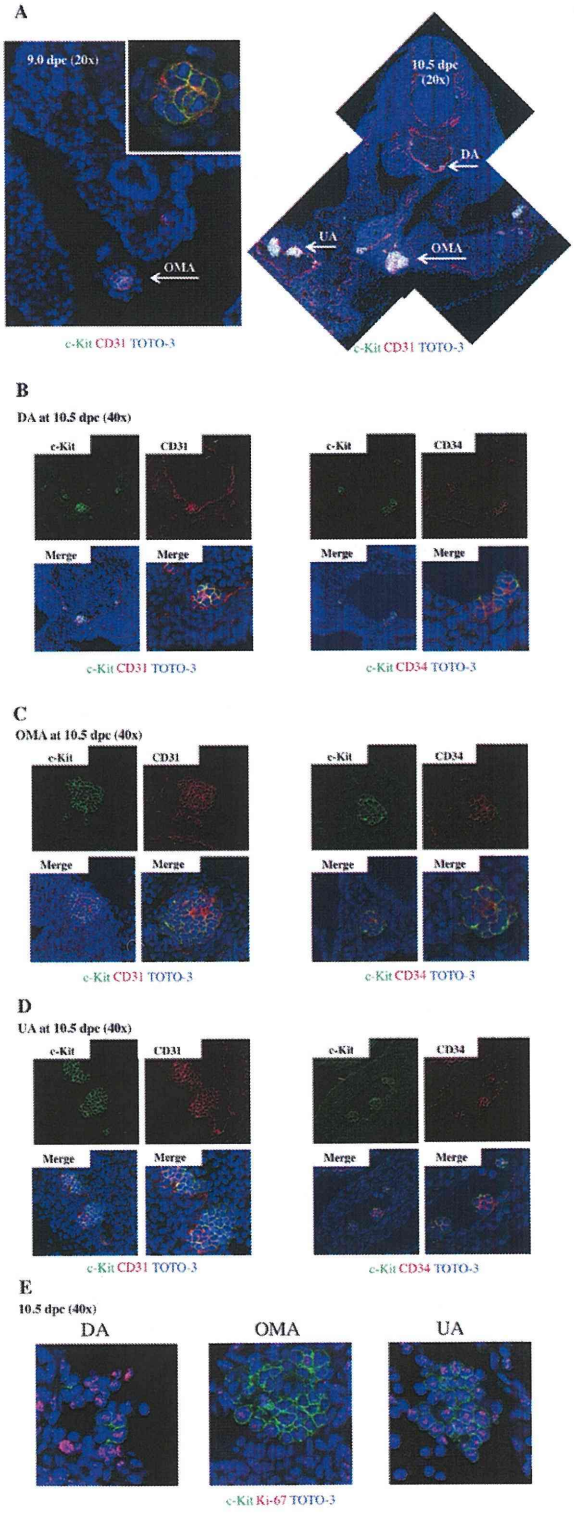

Figure 1. Confocal images of IACs expressing CD31/CD34/c-Kit in the AGM region. Transverse sections of AGM region from ICR mouse embryos at 9.0 and 10.5 dpc were stained with antibodies and observed by confocal microscopy. (**A**) IACs were observed in the omphalomesenteric artery (OMA) at 9.0 dpc (left; magnified view of IACs in upper right panel) and in the OMA, dorsal aorta (DA) and umbilical artery (UA) at 10.5 dpc (right). CD31 (red), c-Kit (green), and TOTO-3 (blue). Arrows indicate IACs. Original magnification is 20x. (**B-D**) IACs were observed in the DA (B), OMA (C) and UA (D) at 10.5 dpc. Left panel shows staining for CD31 (red), c-Kit (green), and TOTO-3 (blue), and right panel shows staining for CD34 (red), c-Kit (green), and TOTO-3 (blue) staining. Images were taken at 40x and zoom was used to show a detail at right lower panel. Another IAC in the DA is shown in Figure S1. (**E**) IACs expressing Ki-67, a marker of proliferation, were observed in the DA (left), OMA (middle) and UA (right). Ki-67 (red), c-Kit (green), and TOTO-3 (blue). Images were taken at 40x and zoom was used to show a detail.
doi:10.1371/journal.pone.0035763.g001

characterization of IACs by flow cytometry and hematopoiesis assays. Here, we demonstrate a significant transition from endothelial to hematopoietic cell phenotype of IAC cells after 9.5 dpc.

Results

Visualization of IACs in mouse embryos

Previous studies identified intra-aortic/arterial clusters (IACs) primarily by immunocytochemistry and microscopy [3,14–15]. Recently, we successfully visualized hematopoietic cell clusters in mouse placenta using thick (20 μm) cryo-sections and antibodies recognizing the embryonic HSC markers c-Kit, CD31 and CD34 and applied this method to quantifying IACs [26]. Cell aggregates consisting of more than three c-Kit-positive cells were defined as an IAC. Here, we used confocal microscopy to expand upon our previous study and characterize the cell types found within IACs according to c-Kit, CD31 and CD34 expression (Figure 1). The first IACs were observed as spherical structures in the omphalomesentric artery (OMA) at 9.0 dpc (12–14 somite pairs [SP]) (Figure 1A, left). Between 9.5 dpc (18–22 SP) to 10.5 dpc (30–34 SP), large arteries such as the dorsal aorta (DA), OMA and umbilical artery (UA) form [14]. IACs were observed in DA, OMA and UA at 10.5 dpc, and the size of IACs in the OMA and UA was significantly larger than those seen in the DA (Figure 1A, right). Localization of IACs in DA was not restricted to the ventral wall of DA, but rather some IACs were observed at dorsal and lateral sides of the wall (data not shown). All IACs in the DA, OMA and UA at 10.5 dpc simultaneously expressed c-Kit, CD31 and CD34 (Figure 1B-D). IACs expressing c-Kit in the different arteries analyzed were also positive for Ki-67, a marker of cell proliferation, regardless of location, suggesting that cells within IACs are highly proliferative (Figure 1E).

Characterization of IACs by flow cytometry and hematopoietic progenitor assays

To further characterize IACs, the caudal portion of embryos containing the p-Sp/AGM region was dissociated and analyzed by flow cytometry. At 10.5 dpc, c-Kit$^+$/CD31$^+$/CD34$^+$ cells, which are equivalent to IACs, were assessed for expression of the cell surface markers VE-cadherin/CD144 (an endothelial cell marker), CD41 (the earliest hematopoietic cell marker), CD45 (a pan-leukocyte marker), Sca-1 (a late fetal and adult HSC marker) and CD150 and EPCR (adult HSC markers) (Figure 2A-H). c-Kit$^+$/CD31$^+$/CD34$^+$ cells represented 0.069±0.01% in whole caudal portion of embryos. Among c-Kit$^+$/CD31$^+$/CD34$^+$ cells, VE-cadherin surface antigen expression decreased significantly within 24 hours from 9.5 to 10.5 dpc. Concomitantly, expression of the hematopoietic markers CD41 and CD45 increased from negative or low levels of expression on IAC cells at 9.5 dpc to abundant

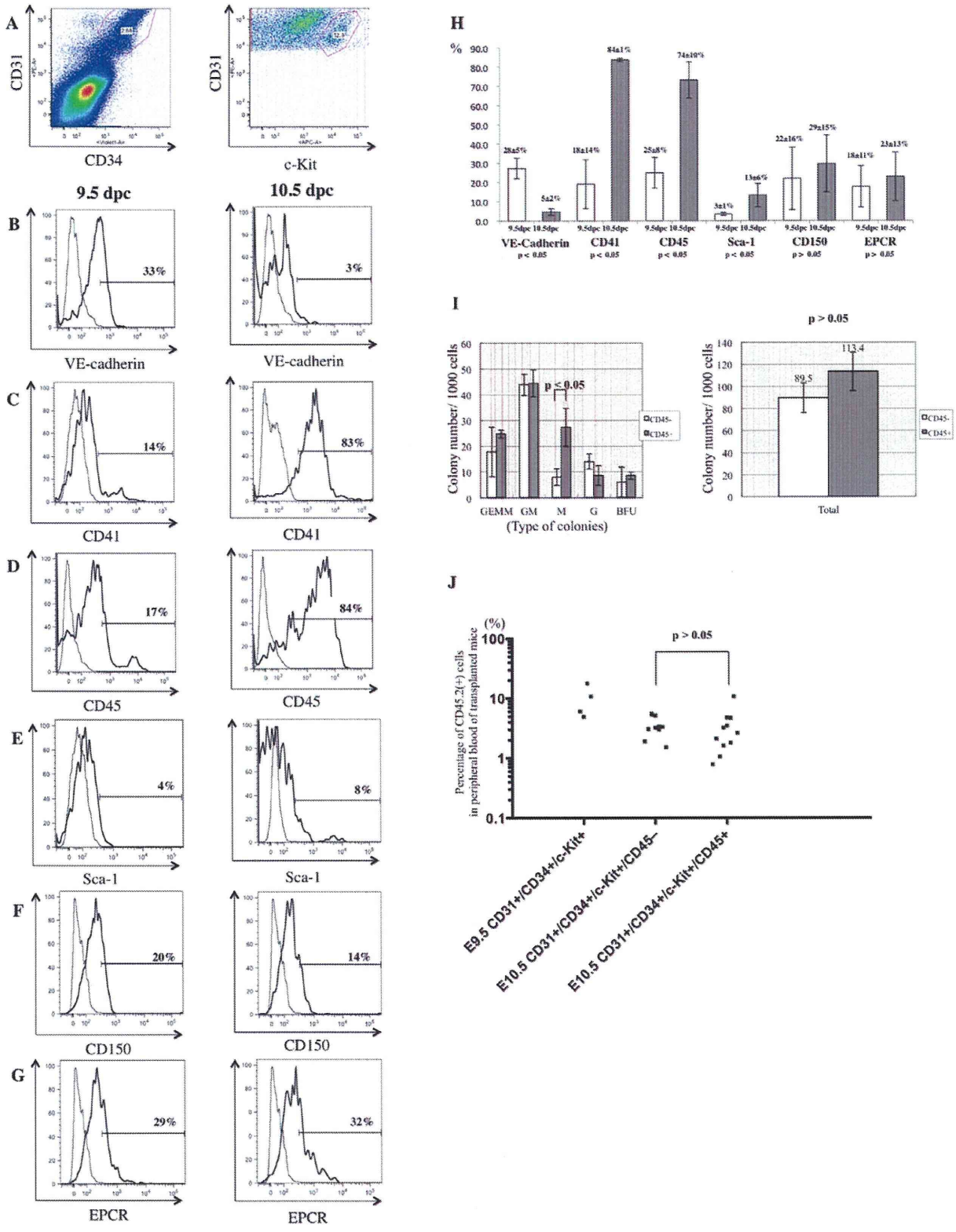

Figure 2. Flow cytometric analysis of CD31$^+$/CD34$^+$/c-Kit$^+$ AGM cells using surface expression of hematopoietic and endothelial cell markers. Single cell suspensions of the caudal portion of embryos containing the p-Sp/AGM region at 9.5 and 10.5 dpc were prepared and analyzed by flow cytometry. (**A**) Cells expressing CD31, CD34 and c-Kit markers of IACs were gated first. Isotype control of flow cytometric analysis is shown in

Figure S2. (**B-G**) Expression of hematopoietic and endothelial cell markers was analyzed on CD31$^+$/CD34$^+$/c-Kit$^+$ cells at 9.5 dpc (left) and 10.5 dpc (right) with the following antibodies: (**B**) VE-cadherin/CD144 (an endothelial cell marker), (**C**) CD41 (the earliest hematopoietic cell marker), (**D**) CD45 (a pan-leukocyte marker), (**E**) Sca-1 (a late fetal and adult HSC marker), (**F**) CD150 and (**G**) EPCR (adult HSC markers). At least 1,000 cells were assessed for each surface antigen. Representative profiles are shown. (**H**) Percentage of expression was summarized. At least 3 independent experiments were performed. Mean ± 2SD was calculated and shown at the top of bars. (**I**) One thousand sorted CD45-negative or CD45-positive CD31$^+$/CD34$^+$/c-Kit$^+$ cells were cultured in semisolid medium containing the hematopoietic cytokines, SCF (Stem Cell Factor), IL (Interleukin)-3, IL-6 and EPO (Erythropoietin). Left and right panels show each fraction and the total number of colonies, respectively. GEMM (colony-forming units of granulocyte erythrocyte monocyte macrophages); GM (of granulocyte macrophages); M (of macrophages); G (of granulocytes); BFU (burst forming units of erythroid cells). (**J**) 50–100 sorted CD31$^+$/CD34$^+$/c-Kit$^+$ cells at 9.5 dpc, as well as CD45-negative and CD45-positive CD31$^+$/CD34$^+$/c-Kit$^+$ cells were transplanted into busulfan-treated Ly5.1 mouse neonates. Approximately one year after transplantation, blood samples were collected and analyzed for CD45.2 expression by flow cytometry. Representative profile of flow cytometric analysis and its negative and positive controls are shown in Figure S3 and S6, respectively.
doi:10.1371/journal.pone.0035763.g002

levels at 10.5 dpc. Sca-1 expression also increased from 9.5 to 10.5 dpc.

We next separated c-Kit$^+$/CD31$^+$/CD34$^+$ cells based on CD45 expression by flow cytometry and performed colony assays and transplantation assays. As shown in Figure 2I (left), the number of CFU-M generated from CD45-positive c-Kit$^+$/CD31$^+$/CD34$^+$ cells (27.3) was significantly higher than CFU-M from CD45-negative c-Kit$^+$/CD31$^+$/CD34$^+$ cells (8.0) ($p<0.05$). However, the total number of hematopoietic colonies did not differ between CD45-negative and CD45-positive c-Kit$^+$/CD31$^+$/CD34$^+$ cells ($p>0.05$). When 50–100 c-Kit$^+$/CD31$^+$/CD34$^+$ cells were transplanted into neonate recipients, there was no significant difference in reconstitution ability (CD45-negative, 3.55%; CD45-positive 3.07%) ($p>0.05$) (Figure 2J). c-Kit$^+$/CD31$^+$/CD34$^+$ cells at 9.5 dpc were able to reconstitute recipients and chimerism to 9.89% was achieved. Presumptive ancestor cells of HSC can reportedly reconstitute neonate recipients but not adult recipients [13]. In addition, pre-HSCs at 10.5 dpc rarely reconstitute adult recipients without culture step [7–9,11]. When 100 c-Kit$^+$/CD31$^+$/CD34$^+$ cells were transplanted into adult recipients, no reconstitution was observed (data not shown).

Expression of CD45 in mouse and human intra-aortic/arterial clusters

CD45-negative and CD45-positive c-Kit$^+$/CD31$^+$/CD34$^+$ cells showed no difference in hematopoietic potential except within the macrophage lineage. To further investigate a role of CD45 expression on c-Kit$^+$/CD31$^+$/CD34$^+$ cells, we used flow cytometry to segregate c-Kit$^+$/CD31$^+$/CD34$^+$ cells into three fractions. Three distinct populations became apparent; CD45negative cells, CD45low cells, and CD45high cells (Figure 3A). The proportion of CD45-negative and CD45-low positive c-Kit$^+$/CD31$^+$/CD34$^+$ cells was higher at 9.5 dpc than at 10.5 dpc, whereas the percentage of CD45-high positive c-Kit$^+$/CD31$^+$/CD34$^+$ cells increased by 5-fold at 10.5 dpc (31.0%) compared to 9.5 dpc (6.3%) (Figure 3B). These data suggest that CD45-negative c-Kit$^+$/CD31$^+$/CD34$^+$ cells are precursors of CD45-high positive c-Kit$^+$/CD31$^+$/CD34$^+$ cells and that CD45 is a marker of IAC maturation. To address this issue, we examined expression levels of the gene encoding CD45 (*Ptprc; protein tyrosine phosphatase, receptor type, C*) and of various hematopoietic transcription factors (Runx1, c-Myb, Evi-1, SCL and Gata2) (Figure 3C-H). CD45-negative c-Kit$^+$/CD31$^+$/CD34$^+$ cells expressed low levels of *CD45* mRNA. *Ptprc* transcript levels increased significantly as CD45 surface protein expression was up-regulated in the c-Kit$^+$/CD31$^+$/CD34$^+$ population. Expression levels of all hematopoietic transcription factor genes assayed except *Evi-1* was highest in CD45-low positive c-Kit$^+$/CD31$^+$/CD34$^+$ cells. In agreement with flow cytometric analysis, evaluation of CD45 protein expression by immunohistochemistry indicated that IACs in the OMA at 9.5 dpc were CD45-negative while some IACs in the DA, OMA and UA were CD45-positive by 10.5 dpc (Figure 4A-D).

IAC formation in the developing human embryo is poorly defined. Having defined the developmental progression of IAC in the mouse above, we next examined IAC morphology and phenotype in a 32 day-old human embryo. Immunohistochemistry of embryonic human cryosections was performed using anti-human CD34 and CD45 antibodies. As shown in Figure 4E, IACs can be detected in ventral wall of the dorsal aorta. CD34 was expressed by a wide range of vascular endothelial cells throughout the embryo. CD45 was restricted to round and in many cases clearly circulating cells. However, within the IAC observable on the ventral wall of the dorsal aorta, cells expressing both CD34 and CD45 can be seen. This reflects the expression pattern we have identified in embryonic mouse IACs.

Transcription factor hierarchy in IAC development

We next observed IAC formation by immunohistochemistry and flow cytometry in mouse embryos harboring mutations associated with aberrant embryonic hematopoiesis [27–32]. Immunohistochemical analysis of *Runx1*$^{-/-}$ embryos lacked IACs in the DA, OMA and UA. Flow cytometric analyses confirmed the absence of c-Kit$^+$/CD31$^+$/CD34$^+$ cells in *Runx1*$^{-/-}$ embryos compared to wild type embryos (Figure 5A-B). *Evi-1*$^{-/-}$ embryos also lacked IACs in the DA, OMA and UA by immunohistochemistry. However, a small frequency of c-Kit$^+$/CD31$^+$/CD34$^+$ cells could be detected by flow cytometry (Figure 5C). In *c-Myb*$^{-/-}$ embryos, IACs were observed at the DA, OMA and UA, and c-Kit$^+$/CD31$^+$/CD34$^+$ cells were also observed by flow cytometry (Figure 5D). Collectively, these results demonstrate that Runx1 is essential for IAC formation while Evi-1 appears to be playing a function downstream of Runx1 in this process.

Discussion

During embryogenesis, a unique cell biological shift takes places in which endothelial cells with adherens junctions detach from each other, alter gene expression and become hematopoietic cells. This process is limited both anatomically and temporally. We here demonstrated that the transition from endothelial to hematopoietic phenotype of IACs occurs from 9.5 dpc in the mouse embryo, earlier than previously described. Furthermore, we show that IACs are identifiable in the human embryo based on CD45 expression, implying that this process in mice is applicable to human.

Previously, we reported an immunohistochemistry visualization technique revealing hematopoietic cell clusters in placenta using thick (20 μm) cryo-sections and antibodies recognizing embryonic HSC markers [26]. Here, we applied this technique to obtain high quality confocal images of intra-aortic/arterial clusters (IACs) in the AGM region. We defined IACs as c-Kit$^+$/CD31$^+$/CD34$^+$ cells. Recently, c-Kit$^+$/CD31$^+$/SSEA-1$^-$ cells were also identified in the AGM region [11]. As CD31 is expressed on both IACs and primordial germ cells (PGCs), it was necessary to exclude PGCs according to SSEA-1 expression. As shown in Figure 2 and 5, we

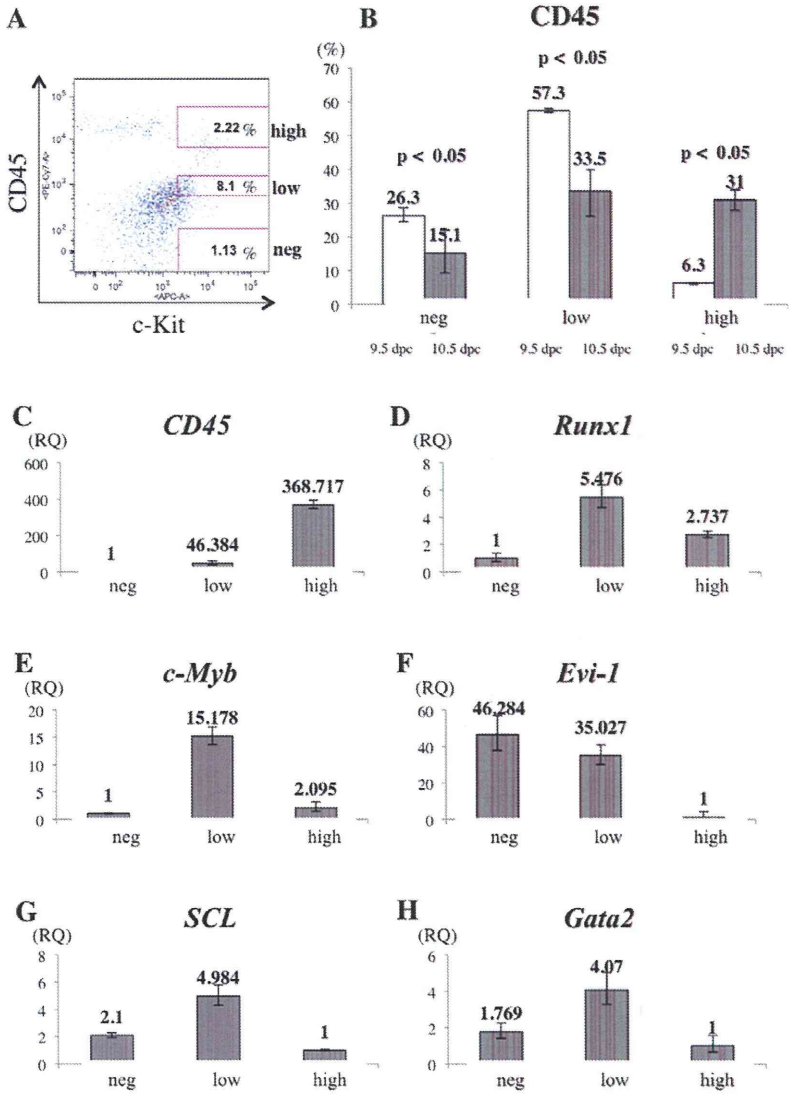

Figure 3. Gene expression analysis in CD31$^+$/CD34$^+$/c-Kit$^+$ AGM cells separated by CD45 expression. (**A**) Single cell suspensions of the caudal portion of embryos containing the AGM region at 10.5 dpc were prepared and analyzed by flow cytometry. Cells expressing CD31 and CD34, IAC markers, were first gated. The profile shows expression of c-Kit (x-axis) and CD45 (y-axis) in CD31$^+$/CD34$^+$ AGM cells (left). Based on intensity of CD45 expression, CD31$^+$/CD34$^+$/c-Kit$^+$ AGM cells were separated into three fractions, CD45-negative (under 10^2 of CD45-fluorescence, same as negative control), -low positive (from $10^{2.5}$ to $10^{3.5}$ of CD45-fluorescence), and -high positive (approximately over 10^4 of CD45-fluorescence). Isotype control and compensation samples of flow cytometric analysis are shown in Figure S4 and S5. (**B**) The percentage of CD45-negative, -low positive, and -high positive c-Kit$^+$/CD31$^+$/CD34$^+$ AGM cells was calculated both at 9.5 dpc (white bars) and 10.5 dpc (black bars). (**C-H**) Gene expression of *CD45* (C), *Runx1* (D), *c-Myb* (E), *Evi-1* (F), *SCL* (G) and *Gata2* (H) was analyzed in sorted CD45-negative, -low positive and -high positive c-Kit$^+$/CD31$^+$/CD34$^+$ AGM cells. Expression levels of *CD45* mRNA are up-regulated as c-Kit$^+$/CD31$^+$/CD34$^+$ cells express CD45 surface protein. Expression levels of *Runx1*, *c-Myb*, *Evi-1*, *SCL* and *Gata2* were highest in CD45-low positive c-Kit$^+$/CD31$^+$/CD34$^+$ cells, whereas that of *Evi-1* was highest in CD45-negative c-Kit$^+$/CD31$^+$/CD34$^+$ cells. RQ represents relative quantity of template in the original sample.
doi:10.1371/journal.pone.0035763.g003

could observe a small number of CD31$^+$/CD34$^-$ cells, which are likely to be PGCs. Since PGCs do not express CD34 at this stage, we could positively select the IAC fraction based on our definition by flow cytometry [33]. Our observation of IACs is compatible with the result showing large IACs were primarily observed in omphalomesentric artery (OMA) and umbilical artery (UA) at 10.5 dpc [11]. In the mouse, IACs protruding into the lumen of arteries were previously reported at 9.5 dpc in studies using microscopy and Tie-2 immunohistochemistry [14,34]. Prior to 9.5 dpc, we identified the first IACs, which formed a spherical structure, in the OMA at 9.0 dpc (Figure 1A). The OMA appears at 8.0 dpc and directly connects with the dorsal aorta (DA). The OMA anastomoses with the DA after 9.5 dpc and loses its connection with the UA by 10.5 dpc [14,35]. Our data (Figure 1E) indicate that IACs are proliferative, based on Ki-67 staining. Taken together, it is likely that the first IACs in the OMA proliferate and are distributed into

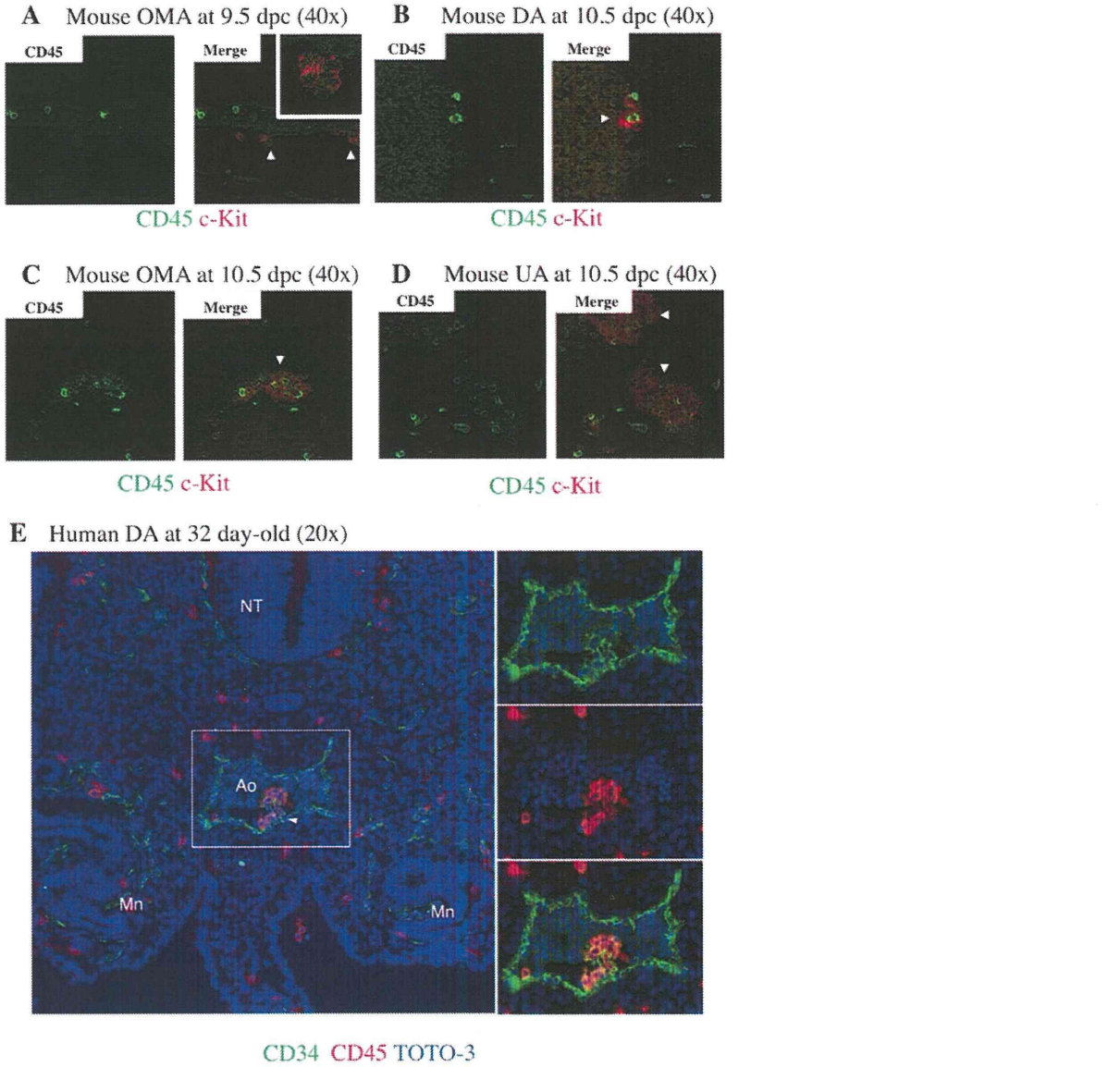

Figure 4. Expression of CD45 by mouse and human IACs. Transverse sections of AGM region were made from ICR mouse embryos at 9.5 and 10.5 dpc and from human embryos at 32 day-old, according to the Carnegie classification, stained with antibodies and observed by confocal microscopy. Arrowheads indicate IACs. (**A**) Mouse IACs in the omphalomesenteric artery (OMA) at 9.5 dpc expressed c-Kit, but not CD45. CD45 (green) and c-Kit (red). Magnified view of IACs is shown at right upper panel in Merge panel. Original magnification is 40x. (**B-D**) Mouse IACs in the dorsal aorta (DA) (B), OMA (C) and umbilical artery (UA) (D) at 10.5 dpc expressed c-Kit, and some expressed CD45. CD45 (green) and c-Kit (red). Original magnification is 40x. (**E**) All human IACs in the DA expressed CD34, and some expressed CD45. CD34 (green), CD45 (red) and TOTO-3 (blue). NT (Neural Tube); Ao (Aorta); Mn (Mesonephros). Original magnification is 20x.
doi:10.1371/journal.pone.0035763.g004

large arteries, such as the DA and UA, as the arterial system develops. Although several reports provide direct evidence that endothelial cells (ECs) generate IACs, we cannot rule out the possibility that either mesodermal cells, the ancestors of hematopoietic cells, or so-called hemangioblasts, which give rise both to ECs and hematopoietic cells, generate IACs by another pathway [17–25]. When VE-cadherin^{+}/CD45^{-} cells were sorted out from AGM regions at 10.5 dpc, and co-aggregated with OP9 stromal cells, these cells acquired HSC activity [8]. As embryos develop, VE-cadherin^{+}/CD45^{+} cells from AGM regions at 11.5 dpc can reconstitute adult recipients without culture step, whereas both VE-cadherin^{+}/CD45$^{+/-}$ cells can after aggregation culture with OP9 stromal cells. It suggests that the transition from endothelial to hematopoietic phenotype in pre-HSCs occurs between 10.5 and 11.5 dpc. According to our flow cytometric analysis of IACs, the transition from endothelial to hematopoietic phenotype occurs after 9.5 dpc (Figure 2). Although we found that 33% of c-Kit^{+}/CD31^{+}/CD34^{+} cells at 9.5 dpc express VE-cadherin, most IACs defined as

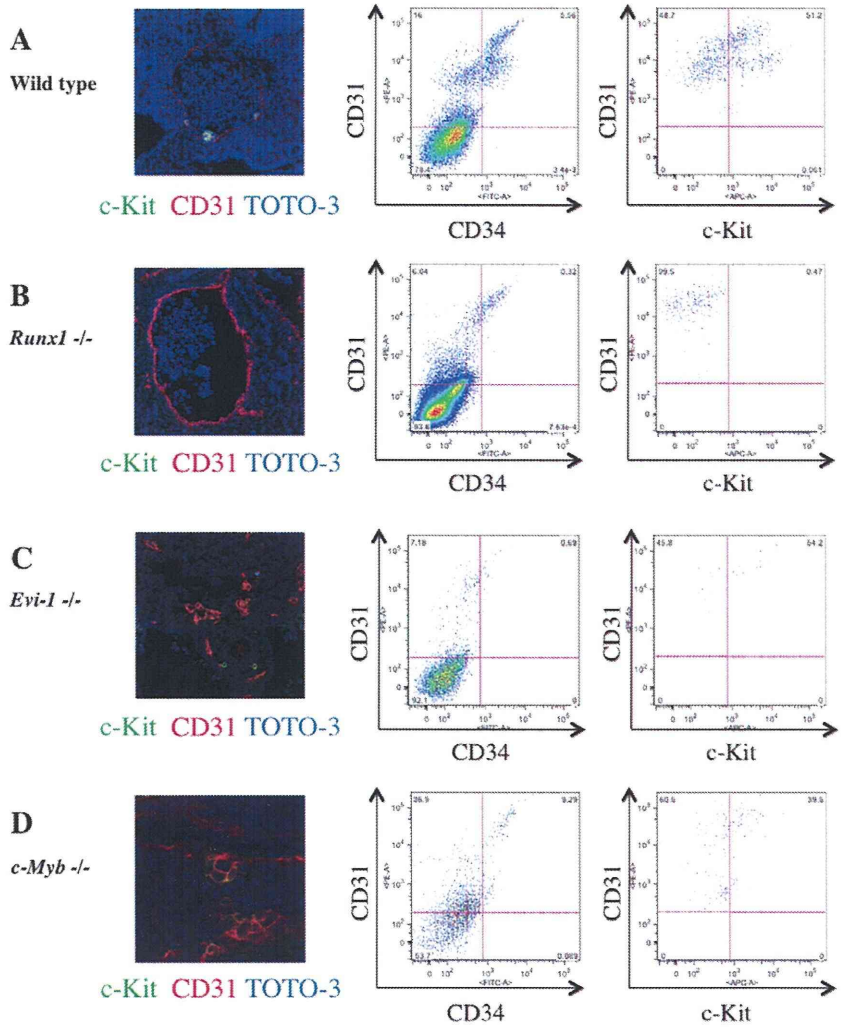

Figure 5. Altered IAC phenotype in *Runx1*$^{-/-}$, *Evi-1*$^{-/-}$ and *c-Myb*$^{-/-}$ embryos. Transverse sections of the AGM region were made from ICR, *Runx1*$^{-/-}$, *Evi-1*$^{-/-}$ and *c-Myb*$^{-/-}$ mouse embryos at 10.5 dpc, stained with antibodies and observed by confocal microscopy. Single cell suspensions of AGM regions from these embryos at 10.5 dpc were prepared and analyzed by flow cytometry. (**A-D**) Left panels show confocal images stained with anti-c-Kit (green) and CD31 (red) antibodies and TOTO-3 (blue). Middle and right panels show flow cytometric profiles of CD34 (x-axis) and CD31 (y-axis), and c-Kit (x-axis) and CD31 (y-axis), respectively. Isotype control and compensation samples of flow cytometric analysis are shown in Figure S2 and S5. (**A**) ICR mouse embryos serve as (wild type) controls. IACs and CD31^{+}/CD34^{+}/c-Kit^{+} AGM cells were observed. (**B**) No IACs were observed in *Runx1*$^{-/-}$ embryos, whereas the aortic structure was conserved (left). No CD31^{+}/CD34^{+}/c-Kit^{+} AGM cells were observed, whereas CD31^{+}/CD34^{+}/c-Kit^{-} AGM cells, which are equivalent to ECs, were observed (middle and right). (**C**) No IACs were observed and aortic structure was altered in *Evi-1*$^{-/-}$ embryos (left). CD31^{+} AGM cells were observed, but they did not express CD34 and c-Kit (middle and right). (**D**) IACs were observed in *c-Myb*$^{-/-}$ embryos and the aortic structure was conserved (left). CD31^{+}/CD34^{+}/c-Kit^{+} AGM cells were observed (middle and right).
doi:10.1371/journal.pone.0035763.g005

c-Kit^{+}/CD31^{+}/CD34^{+} cells by flow cytometry did not contribute to blood vessel structure. VE-cadherin is expressed in IACs as well as in ECs [16]. It is likely that sorted VE-cadherin^{+}/CD45^{-} cells from AGM regions at 10.5 dpc contained ECs with HSC potential in addition to some IACs. Further studies are necessary to determine how ECs contribute to IAC generation. CD150 belongs to the SLAM family and its expression is developmentally regulated on the surface of HSCs. At 11.5 dpc, CD150^{-} cells can reconstitute adult recipients, but CD150^{+} cells not [10]. In this study, CD150 expression was examined on c-Kit^{+}/CD31^{+}/CD34^{+} cells by flow cytometry and the percentage of CD150 expression was not changed (Figure 2F, H). It will be interesting to compare the CD150 expression between 10.5 and 11.5 dpc.

The pan-leukocyte marker CD45 is a transmembrane glycoprotein that functions as a protein phosphotyrosine phosphatase. Although loss of the *CD45* gene results in T and B lymphocyte anomalies in adult, there appears to be no significant abnormality in HSC development during embryogenesis [36–38]. We observed that CD45 protein expression was up-regulated in c-Kit^{+}/CD31^{+}/CD34^{+} cells between 9.5 and 10.5 dpc (Figure 2D). Our results are compatible with the report showing that CD45 is expressed on the surface of IACs at 10.5 dpc, but not on the IACs at 9.5 dpc [11].

In agreement with previous reports, we observed no significant differences in HSC activity based on neonatal transplantation, whereas myeloid potential differs based on colony formation assay between CD45-negative and CD45-positive c-Kit$^+$/CD31$^+$/CD34$^+$ cells, suggesting that CD45 expression is not required for hematopoietic cell identity (Figure 2I, J) [39–40]. However, pre-HSCs that can reconstitute both adult and neonatal recipients appear at 10.5 dpc, whereas presumptive ancestor cells of HSC that can reconstitute only neonatal but not adult recipients appear at 9.5 dpc [7,12–13]. In accordance with flow cytometric data, some IACs expressed CD45 while others did not in both 10.5 dpc mouse embryos and 32 day-old human embryos (Figure 4B-E). Taken together, although CD45 does not function in HSC development, its expression on the cell surface might serve as a marker of pre-HSC maturation from ancestor cells of HSC. With regard to myeloid potential, only macrophage development differs (Figure 2I). At 10.5 dpc, macrophages are reportedly c-Kit$^-$/CD31$^-$/CD45$^+$ cells, and we could observe some c-Kit$^-$/CD45$^+$ cells in the AGM regions (Figure 4) [11]. CD45 expression on c-Kit$^+$/CD31$^+$/CD34$^+$ cells might be the diverging point of myeloid potential. Furthermore, we identified *CD45* gene expression in CD45-negative c-Kit$^+$/CD31$^+$/CD34$^+$ cells, suggesting that these cells are primed to differentiate into CD45-positive c-Kit$^+$/CD31$^+$/CD34$^+$ cells. Expression levels of *Runx1, c-Myb, SCL* and *Gata2* were highest in CD45-low positive c-Kit$^+$/CD31$^+$/CD34$^+$ cells, implying that the transition from endothelial to hematopoietic phenotype of IACs occurs in CD45-low positive c-Kit$^+$/CD31$^+$/CD34$^+$ cells, as these transcription factors are reportedly important for the switch to hematopoietic cells [22]. Evi-1 is involved in vasculo-angiogenesis in addition to HSC development [31]. Therefore, high expression level of *Evi-1* gene in CD45-negative c-Kit$^+$/CD31$^+$/CD34$^+$ cells implies that this population still preserves some endothelial identity.

We also investigated IACs from *Runx1*$^{-/-}$, *Evi-1*$^{-/-}$ or *c-Myb*$^{-/-}$ mouse embryos. Runx1 is essential for definitive hematopoiesis, and its expression marks the site of *de novo* generation of definitive hematopoietic cells [28–30]. In agreement with previous reports, we observed an absence of IACs in *Runx1*$^{-/-}$ mouse embryos. *Evi-1*$^{-/-}$ mouse embryos displayed abnormalities in vascular and hematopoietic development [31–32]. As shown in Figure 5C, *Evi-1*$^{-/-}$ mouse embryos comprised a few c-Kit$^+$/CD31$^+$/CD34$^+$ cells based on flow cytometric analysis. High expression of *Evi-1* in CD45-negative c-Kit$^+$/CD31$^+$/CD34$^+$ cells may correlate with vascular development and impairment of IAC formation. c-Myb is essential for HSC maturation and proliferation, and *c-Myb*$^{-/-}$ mouse embryos die at 15.5 dpc from impaired definitive hematopoiesis in fetal liver, although primitive hematopoiesis appears normal [27]. In contrast to *Runx1*$^{-/-}$ or *Evi-1*$^{-/-}$ mouse embryos, *c-Myb*$^{-/-}$ mouse embryos exhibited IACs.

Several evidences reveal that HSCs are generated from ECs [17–21]. Taken together, our results corroborate HSC-generation from ECs and imply that IACs gradually acquire hematopoietic phenotype after 9.5 dpc. Understanding how IACs are generated could lead to an understanding of how to manipulate HSC generation from ES/iPS cells and thus be applicable to future clinical applications.

Materials and Methods

Mice

Ly5.1 (Sankyo Labo Service, Tokyo, Japan) mice, Ly5.2 adult C57/BL6 mice (Kyudo, Tosu, Japan), ICR mice (SLC, Hamamatsu, Japan), *Runx1*$^{+/-}$ mice (provided by Dr. Speck at University of Pennsylvania), *Evi-1*$^{+/-}$ mice (JAX mice and Services, Bar Harbor, ME) and *c-Myb*$^{+/-}$ mice (JAX mice and Services) were used in these studies. To analyze cells, pregnant mice were sacrificed at 9.0–10.5 dpc and somite pair number was counted. Embryos at 9.0 dpc with 12–14 somite pairs (SP), 9.5 dpc with 18–22 SP and 10.5 dpc with 30–34 SP were dissected out, respectively. Animals were handled according to the Guidelines for the Care and Use of Laboratory Animals of Kyushu University. This study was approved by Animal Care and Use Committee, Kyushu University (Approval ID: A21-068-0).

Mouse immunohistochemistry

Embryos were dissected out and fixed in 2% paraformaldehyde in PBS, followed by equilibration in 30% sucrose in PBS. Embryos were embedded in OCT compound (SAKURA, Tokyo, Japan) and frozen in liquid nitrogen. Tissues were sliced at 20 μm on a Leica CM1900 UV cryostat, transferred to glass slides (Matsunami, Osaka, Japan) and dried thoroughly. Sections were blocked in 1% BSA in PBS and incubated in PBS containing 1% BSA with appropriate dilutions of the following primary antibodies: goat anti-mouse c-Kit (R&D Systems, Minneapolis, MN), rat anti-mouse CD31 (BD Biosciences, San Diego, CA), rat anti-mouse CD34 (BD Biosciences), rat anti-mouse CD45 (Biolegend) and rat anti-mouse Ki-67 antigen (Dako Corporation, Carpinteria, CA) at 4°C overnight. After washing in PBS three times, sections were incubated with appropriate dilutions of the following secondary antibodies: Alexa Fluor 488 donkey anti-rat IgG (Invitrogen, Carlsbad, CA), Alexa Fluor 488 donkey anti-goat IgG (Invitrogen), Alexa Fluor 546 donkey anti-goat IgG (Invitrogen) and Alexa Fluor 568 donkey anti-goat IgG (Invitrogen), as well as TOTO-3 (Invitrogen) to stain nuclei, at room temperature for 30 minutes. Samples were mounted on coverslips using fluorescent mounting medium (Dako Corporation) and assessed using a FluoView 1000 confocal microscope (Olympus, Tokyo, Japan).

Human tissues

Human embryos were obtained from voluntary abortions performed according to guidelines and with the approval of the French National Ethics Committee. In all cases, written consent allowing use of the embryo for research was obtained from the patient. Developmental age was estimated based on anatomical criteria and the Carnegie classification as previously described [41–42].

Human immunohistochemistry

Embryos were fixed overnight at 4°C in PBS plus 4% paraformaldehyde (Sigma-Aldrich), rinsed twice in PBS, then in PBS/15% sucrose (Sigma-Aldrich) for at least 24 hours. Tissues were then embedded in PBS with 15% sucrose and 7.5% gelatin (Sigma-Aldrich), frozen and stored at -80°C. Frozen sections (5 μm) were stored at −20°C until use, and then thawed and hydrated in PBS [37]. For double-staining, the TSA Plus Fluorescence amplification system was used, according to the manufacturer's instructions (NEN-Perkin Elmer). Endogenous peroxidases were inhibited for 20 minutes in PBS containing 0.2% hydrogen peroxide (Sigma-Aldrich). Sections were washed in PBS and non-specific binding sites were blocked with PBS/5% goat serum (Vector Laboratories) for 1 hour. Sections were then incubated with uncoupled antibody to CD45 (overnight at room temperature). After rinsing, sections were incubated with biotinylated goat anti-mouse IgG antibody (Immunotech) for 1 hour and then with peroxidase-labeled streptavidin (Immunotech) for 1 hour. Staining was revealed using fluorescent tyramide (TMR, Tetramethylrhodamine). Residual peroxidase activity was inhibited in PBS/0.2% hydrogen peroxide for 10 min at RT. After 3

washings in PBS, slides were treated with an Avidin/Biotin blocking kit according to the manufacturer's instructions (Vector Laboratories). Sections were washed and incubated with anti-CD34 antibody at room temperature for 2 hours, then with biotinylated goat anti-mouse IgG antibody (Immunotech) for 1 hour at RT, and with Alexa 488-labeled streptavidin for 1 hour. Slides were mounted in Vectashield medium (Vector Laboratories). Monoclonal antibodies to CD34 (IgG1, clone Qbend-10) and CD45 (IgG1, clone Hle-1) were purchased from Immunotech and Becton-Dickinson Biosciences, respectively.

Cell preparation

The caudal portion of embryos containing the p-Sp/AGM region was used to obtain a single cell suspension. Tissues were incubated with 1 mg/ml collagenase in medium supplemented with 10% fetal bovine serum for 30 minutes at 37°C and filtered through 40-μm nylon cell strainers (BD Biosciences).

Flow cytometry and cell sorting

Antibodies used for analysis were: FITC-conjugated anti-mouse CD41 (eBioscience, San Diego, CA), FITC-conjugated anti-mouse Sca-1 (eBioscience), FITC-conjugated anti-mouse EPCR (Endothelial Protein C Receptor) known as CD201 (Stem Cell Technologies inc, Vancouver, BC), PE-conjugated anti-mouse CD31 (BD Biosciences), PE-Cy7-conjugated anti-mouse CD45 (BioLegend), APC and APC-Cy7-conjugated anti-mouse c-Kit (BD Biosciences), Aexa Fluor488-conjugated anti-mouse CD150 (BioLegend), APC-conjugated anti-mouse VE-cadherin (clone name; VECD-1, provided by Dr. Ogawa at Kumamoto University), and FITC and Pacific Blue-conjugated anti-mouse CD34 (eBioscience). Flow cytometric analysis and cell sorting were carried out using a FACSAria SORP cell sorter (BDIS, San Jose, CA). Data files were analyzed using FlowJo software (Tree Star, Inc., San Carlos, CA).

RNA extraction and real-time PCR analysis

Total RNA was isolated using the RNAqueous 4PCR kit (Ambion Inc., Austin, Texas). mRNA was reverse transcribed using a High-Capacity RNA-to-cDNA kit (Life Technologies, Carlsbad, CA). The quality of cDNA synthesis was evaluated by amplifying mouse ß-actin using PCR. Thirty thermal cycles were used as follows: denaturation at 95°C for 10 sec, annealing at 60°C for 20 sec, followed by extension at 72°C for 20 seconds. Gene expression levels were measured by real time PCR with TaqMan® Gene Expression Master Mix and StepOnePlus™ real time PCR (Life Technologies). All probes were from TaqMan® Gene Expression Assays (Life Technologies). All analyses were performed in triplicate wells; mRNA levels were normalized to ß-actin and the relative quantity (RQ) of expression was compared with a reference sample.

Colony formation assay

Sorted cells were suspended in 3 ml of MethoCult® GF M3434 (Stemcell Technologies) distributed into three 35 mm dishes and then incubated in 5% CO_2 at 37°C. Colonies were counted up 14 days later using an inverted phase contrast microscope CKX41 (Olympus, Tokyo, Japan).

Transplantation assay

To examine neonatal repopulating HSCs, sorted cells were transplanted into busulfan-treated Ly5.1 mouse neonates as described previously [9,15]. Briefly, time-pregnant mice were injected on days 17 and 18 after conception with 15 μg of busulfan/gram body weight of the mother (Sigma-Aldrich, St.Louis MO). Isolated cells were suspended in 25 μl PBS and transplanted into neonates at the time of delivery using a 100 μl Hamilton syringe (Hamilton, Reno, NV). Approximately one year after transplantation, blood samples were collected, lysed in BD Pharm Lyse (BD Biosciences) and analyzed for CD45.2 expression by flow cytometry.

Supporting Information

Figure S1 Additional confocal images of IAC expressing CD31/CD34/c-Kit in the dorsal aorta of AGM region at 10.5 dpc. Staining for CD34 (red), c-Kit (green), and TOTO-3 (blue) is shown. Original magnification is 40x.
(TIFF)

Figure S2 Single cell suspensions of the caudal portion of embryos containing the p-Sp/AGM region at 9.5 and 10.5 dpc were prepared and analyzed by flow cytometry. Upper panels show isotype control of analysis corresponding to Figure 2A. Lower panels show isotype control of analysis corresponding to Figure 5.
(TIFF)

Figure S3 50–100 sorted $CD31^-/CD34^+/c\text{-}Kit^+$ cells at 9.5 dpc, as well as CD45-negative and CD45-positive $CD31^+/CD34^+/c\text{-}Kit^+$ cells were transplanted into busulfan-treated Ly5.1 mouse neonates. Approximately one year after transplantation, blood samples were collected, lysed in lysing solution and analyzed for CD45.2 expression by flow cytometry. Representative profile of flow cytometric analysis is shown.
(TIFF)

Figure S4 Single cell suspensions of the caudal portion of embryos containing the AGM region at 10.5 dpc were prepared and analyzed by flow cytometry. The profile shows isotype control of analysis corresponding to Figure 3A. Based on the isotype control, sorting gates are set into three fractions, CD45-negative (under 10^2 of CD45-fluorescence, same as negative control), -low positive (from $10^{2.5}$ to $10^{3.5}$ of CD45-fluorescence), and -high positive (approximately over 10^4 of CD45-fluorescence).
(TIFF)

Figure S5 Single cell suspensions of the caudal portion of embryos containing the p-Sp/AGM region at 9.5 and 10.5 dpc were prepared and analyzed by flow cytometry. Compensation samples of analysis corresponding to Figure 3A and 5 were shown.
(TIFF)

Figure S6 Negative and positive controls to transplantation analysis are shown corresponding to Figure S3. Peripheral blood samples were obtained from Ly5.1 adult mouse for negative control and Ly5.2 adult C57/BL6 mice for positive control, respectively.
(TIFF)

Acknowledgments

We thank the Research Support Center, the Graduate School of Medical Sciences, Kyushu University for technical support, Drs. K. Nakao and K. Kulkeaw for technical support, and Dr. Elise Lamar for critical reading of our manuscript.

Author Contributions

Conceived and designed the experiments: DS. Performed the experiments: CM KB YH YK MT DS. Analyzed the data: CM SF KB MT DS. Contributed reagents/materials/analysis tools: CM KB MT KT KA DS. Wrote the paper: CM SF DS.

References

1. Dzierzak E, Speck NA (2008) Of lineage and legacy: the development of mammalian hematopoietic stem cells. Nat Immunol 9: 129–136.
2. Mikkola HK, Orkin SH (2006) The journey of developing hematopoietic stem cells. Development 133: 3733–3744.
3. Godin I, Cumano A (2002) The hare and the tortoise: an embryonic haematopoietic race. Nat Rev Immunol 2: 593–604.
4. Dieterlen-Lievre F, Pouget C, Bollerot K, Jaffredo T (2006) Are intra-aortic hemopoietic cells derived from endothelial cells during ontogeny? Trends Cardiovasc Med 16: 128–139.
5. Jaffredo T, Bollerot K, Sugiyama D, Gautier R, Drevon C (2005) Tracing the hemangioblast during embryogenesis: developmental relationships between endothelial and hematopoietic cells. Int J Dev Biol 49: 269–277.
6. Sugiyama D, Tsuji K (2006) Definitive hematopoiesis from endothelial cells in the mouse embryo; a simple guide. Trends Cardiovasc Med 16: 45–49.
7. Medvinsky A, Dzierzak E (1996) Definitive hematopoiesis is autonomously initiated by the AGM region. Cell 86: 897–906.
8. Taoudi S, Gonneau C, Moore K, Sheridan JM, Blackburn CC, et al. (2008) Extensive hematopoietic stem cell generation in the AGM region via maturation of VE-cadherin+CD45+ pre-definitive HSCs. Cell Stem Cell 3: 99–108.
9. Rybtsov S, Sobiesiak M, Taoudi S, Souilhol C, Senserrich J, et al. (2011) Hierarchical organization and early hematopoietic specification of the developing HSC lineage in the AGM region. J Exp Med 208: 1305–1315.
10. McKinney-Freeman SL, Naveiras O, Yates F, Loewer S, Philitas M, et al. (2009) Surface antigen phenotypes of hematopoietic stem cells from embryos and murine embryonic stem cells. Blood 114: 268–278.
11. Yokomizo T, Dzierzak E (2010) Three-dimensional cartography of hematopoietic clusters in the vasculature of whole mouse embryos. Development 137: 3651–3661.
12. Kumano K, Chiba S, Kunisato A, Sata M, Saito T, et al. (2003) Notch1 but not Notch2 is essential for generating hematopoietic stem cells from endothelial cells. Immunity 18: 699–711.
13. Yoder MC, Hiatt K, Dutt P, Mukherjee P, Bodine DM, et al. (1997) Characterization of definitive lymphohematopoietic stem cells in the day 9 murine yolk sac. Immunity 7: 335–344.
14. Garcia-Porrero JA, Godin IE, Dieterlen-Lievre F (1995) Potential intraembryonic hemogenic sites at pre-liver stages in the mouse. Anat Embryol (Berl) 192: 425–435.
15. Garcia-Porrero JA, Manaia A, Jimeno J, Lasky LL, Dieterlen-Lievre F, et al. (1998) Antigenic profiles of endothelial and hemopoietic lineages in murine intraembryonic hemogenic sites. Dev Comp Immunol 22: 303–319.
16. Fraser ST, Ogawa M, Yokomizo T, Ito Y, Nishikawa S (2003) Putative intermediate precursor between hematogenic endothelial cells and blood cells in the developing embryo. Dev Growth Differ 45: 63–75.
17. Jaffredo T, Gautier R, Eichmann A, Dieterlen-Lievre F (1998) Intraaortic hemopoietic cells are derived from endothelial cells during ontogeny. Development 125: 4575–4583.
18. Sugiyama D, Ogawa M, Hirose I, Jaffredo T, Arai K, et al. (2003) Erythropoiesis from acetyl LDL incorporating endothelial cells at the preliver stage. Blood 101: 4733–4738.
19. Sugiyama D, Arai K, Tsuji K (2005) Definitive hematopoiesis from acetyl LDL incorporating endothelial cells in the mouse embryo. Stem Cells Dev 14: 687–696.
20. Bertrand JY, Giroux S, Golub R, Klaine M, Jalil A, et al. (2005) Characterization of purified intraembryonic hematopoietic stem cells as a tool to define their site of origin. Proc Natl Acad Sci U S A 102: 134–139.
21. Zovein AC, Hofmann JJ, Lynch M, French WJ, Turlo KA, et al. (2008) Fate tracing reveals the endothelial origin of hematopoietic stem cells. Cell Stem Cell 3: 625–636.
22. Chen MJ, Yokomizo T, Zeigler BM, Dzierzak E, Speck NA (2009) Runx1 is required for the endothelial to haematopoietic cell transition but not thereafter. Nature 457: 887–891.
23. Bertrand JY, Chi NC, Santoso B, Teng S, Stainier DY, et al. (2010) Haematopoietic stem cells derive directly from aortic endothelium during development. Nature 464: 108–111.
24. Kissa K, Herbomel P (2010) Blood stem cells emerge from aortic endothelium by a novel type of cell transition. Nature 464: 112–115.
25. Boisset JC, van Cappellen W, Andrieu-Soler C, Galjart N, Dzierzak E, et al. (2010) In vivo imaging of haematopoietic cells emerging from the mouse aortic endothelium. Nature 464: 116–120.
26. Sasaki T, Mizuochi C, Horio Y, Nakao K, Akashi K, et al. (2010) Regulation of hematopoietic cell clusters in the placental niche through SCF/Kit signaling in embryonic mouse. Development 137: 3941–3952.
27. Mucenski ML, McLain K, Kier AB, Swerdlow SH, Schreiner CM, et al. (1991) A functional c-myb gene is required for normal murine fetal hepatic hematopoiesis. Cell 65: 677–689.
28. Okuda T, van Deursen J, Hiebert SW, Grosveld G, Downing JR (1996) AML1, the target of multiple chromosomal translocations in human leukemia, is essential for normal fetal liver hematopoiesis. Cell 84: 321–330.
29. Wang Q, Stacy T, Binder M, Marin-Padilla M, Sharpe AH, et al. (1996) Disruption of the Cbfa2 gene causes necrosis and hemorrhaging in the central nervous system and blocks definitive hematopoiesis. Proc Natl Acad Sci U S A 93: 3444–3449.
30. North T, Gu TL, Stacy T, Wang Q, Howard L, et al. (1999) Cbfa2 is required for the formation of intra-aortic hematopoietic clusters. Development 126: 2563–2575.
31. Yuasa H, Oike Y, Iwama A, Nishikata I, Sugiyama D, et al. (2005) Oncogenic transcription factor Evi1 regulates hematopoietic stem cell proliferation through GATA-2 expression. EMBO J 24: 1976–1987.
32. Goyama S, Yamamoto G, Shimabe M, Sato T, Ichikawa M, et al. (2008) Evi-1 is a critical regulator for hematopoietic stem cells and transformed leukemic cells. Cell Stem Cell 3: 207–220.
33. Wood HB, May G, Healy L, Enver T, Morris-Kay GM (1997) CD34 expression patterns during early mouse development are related to modes of blood vessel formation and reveal additional sites of hematopoiesis. Blood 90: 2300–2311.
34. Takakura N, Huang XL, Naruse T, Hamaguchi I, Dumont DJ, et al. (1998) Critical role of the TIE2 endothelial cell receptor in the development of definitive hematopoiesis. Immunity 9: 677–686.
35. Theiler K (1972) The house mouse: development and normal stages from fertilization to 4 weeks of age. Springer, Berlin Heidelberg New York.
36. Kishihara K, Penninger J, Wallace VA, Kundig TM, Kawai K, et al. (1993) Normal B lymphocyte development but impaired T cell maturation in CD45-exon6 protein tyrosine phosphatase-deficient mice. Cell 74: 143–156.
37. Byth KF, Conroy LA, Howlett S, Smith AJ, May J, et al. (1996) CD45-null transgenic mice reveal a positive regulatory role for CD45 in early thymocyte development, in the selection of CD4+CD8+ thymocytes, and B cell maturation. J Exp Med 183: 1707–1718.
38. Mee PJ, Turner M, Basson MA, Costello PS, Zamoyska R, et al. (1999) Greatly reduced efficiency of both positive and negative selection of thymocytes in CD45 tyrosine phosphatase-deficient mice. Eur J Immunol 29: 2923–2933.
39. North TE, de Bruijn MF, Stacy T, Talebian L, Lind E, et al. (2002) Runx1 expression marks long-term repopulating hematopoietic stem cells in the midgestation mouse embryo. Immunity 16: 661–672.
40. Matsubara A, Iwama A, Yamazaki S, Furuta C, Hirasawa R, et al. (2005) Endomucin, a CD34-like sialomucin, marks hematopoietic stem cells throughout development. J Exp Med 202: 1483–1492.
41. O'Rahilly R, Muller F (1987) Development Stages in Human Embryos. Washington: Carnegie Institution of Washington.
42. Tavian M, Peault B (2005) The changing cellular environments of hematopoiesis in human development in utero. Exp Hematol 33: 1062–1069.

Stem Cell Rev and Rep
DOI 10.1007/s12015-012-9388-1

Mesodermal and Hematopoietic Differentiation from ES and iPS Cells

Tomoko Inoue-Yokoo · Kenzaburo Tani · Daisuke Sugiyama

Abstract Embryonic stem (ES) and induced pluripotent stem (iPS) cells can differentiate into any type of tissue when grown in a suitable culture environment and are considered valuable tools for regenerative medicine. In the field of hematology, generation of hematopoietic stem cells (HSCs) and mature hematopoietic cells (HCs) from ES and iPS cells through mesodermal cells, the ancestors of HCs, can facilitate transplantation and transfusion therapy. Several studies report generation of functional HCs from both mouse and human ES and iPS cells. This approach will likely be applied to individual patient-derived iPS cells for regenerative medicine approaches and drug screening in the future. Here, we summarize current studies of HC-generation from ES and iPS cells.

Keywords Mesoderm induction · Hematopoietic cell differentiation · ES cell · iPS cell

Abbreviations

ES	Embryonic stem
iPS	Induced pluripotent stem
HSC	Hematopoietic stem cell
HPC	Hematopoietic progenitor cell
HC	Hematopoietic cell

T. Inoue-Yokoo · D. Sugiyama (✉)
Division of Hematopoietic Stem Cells, Advanced Medical Initiatives, Department of Advanced Medical Initiatives, Kyushu University Faculty of Medical Sciences, Fukuoka 812-8582, Japan
e-mail: ds-mons@yb3.so-net.ne.jp

T. Inoue-Yokoo
Department of Medicine and Biosystemic Science, Kyushu University Graduate School of Medical Sciences, Fukuoka 812-8582, Japan

K. Tani
Department of Medical Genomics, Medical Institute of Bioregulation, Kyushu University, Fukuoka 812-8582, Japan

Published online: 09 June 2012

Introduction

Hematopoiesis is the process by which mature and functional hematopoietic cells (HCs), such as leukocytes (granulocytes, macrophages, lymphocytes), erythrocytes and platelets, are generated from hematopoietic stem cells (HSCs) and hematopoietic progenitor cells (HPCs) to maintain homeostasis. Hematopoiesis is controlled intrinsically via transcription factors and small RNAs [1–3] and extrinsically through growth factors and extracellular matrices secreted from niche cells surrounding HCs [4–6]. Faulty regulation of hematopoiesis leads to hematological diseases, such as anemia, leukemia and lymphoma, in which HSC transplantation and/or transfusion of erythrocytes or platelets are dependent on disease status. Regardless of the HSC source (patient cells, donor cells, or cord blood cells), transplantation is a promising therapy for some hematological diseases. However, problems remain in HSC transplantation, such as donor shortages, viral contamination and graft-versus host disease. To overcome these problems, HSC generation from other cells is a possible alternative to expansion of cord blood HSCs. Mature HCs, such as erythrocytes and platelets, are obtained primarily from donors and transfused into patients with hematological diseases and under surgical operation. Likewise, use of HSCs is also associated with problems, such as shortage of donors, viral infection and rejection. Overall, the ability to generate mature HCs from other cells would guarantee a continuous supply of cells and ensure safe and efficient transfusion therapy.

To address these issues, in vitro HC generation from other cells, particularly from embryonic stem (ES) cells [7] and induced pluripotent stem (iPS) cells [8], has been attempted. ES cells are established from the inner cell mass of a blastocyst, maintain their pluripotent and undifferentiated status in vitro and differentiate into any cell type in appropriate culture conditions. Furthermore, ES cells can have pluripotency in vivo and form teratoma in immunodeficient mice, and can be used to generate chimeric mice in vivo. To understand molecular mechanisms underlying developmental processes, ES cells are frequently utilized, since they mimic in vivo development in vitro (Fig. 1). iPS cells, on the other hand are created by ectopic expression of four transcription factors (Oct3/4, Sox2, Klf4, and c-Myc) in somatic cells, such as fibroblasts, hepatocytes, gastric epithelial cells, pancreatic cells, B cells and $CD34^+$ cord blood cells, and exhibit properties of pluripotent ES cells. iPS cells established from a patient's somatic cells could function as useful tools for regenerative medicine and drug screening by manipulating lineage specific differentiation in vitro (Fig. 1).

Here we summarize current studies relevant to generation of HCs and mesodermal cells from ES and iPS cells in both mice and humans (Table 1).

General Induction Methods

Several methods to differentiate mesodermal cells and hematopoietic cells from ES and iPS cells have been reported. They include (i) embryoid body (EB) formation, (ii) co-culture with feeder cells, and (iii) growth in extra cellular matrix-coated dishes. In the first method, undifferentiated ES and iPS cell colonies are separated into small cell pieces enzymatically or by physical dissection, following by EB formation in suspension in a culture dish or hanging drop. EBs are spherical cell aggregates that proliferate and differentiate into all three germ layers (i). Alternatively, ES or iPS cells can be seeded on OP9 stromal cells, which are established from the newborn calvaria of op-/op- mice and support HCs differentiation (ii), or seeded on collagen IV-coated dishes, which promote cell proliferation and form

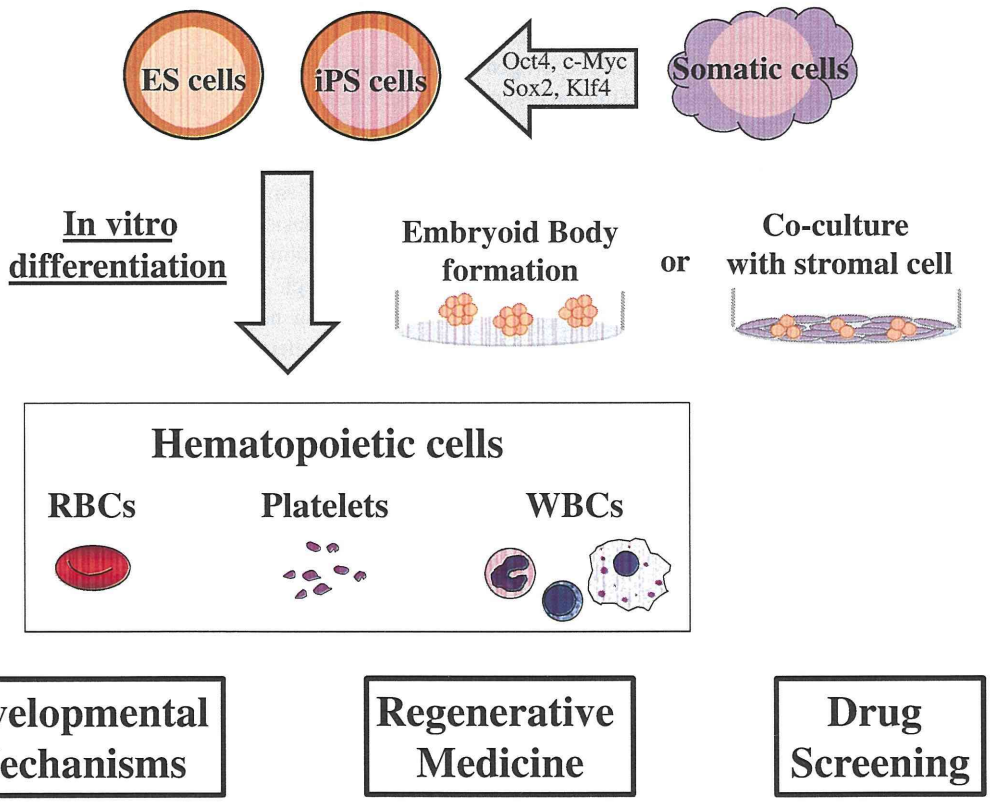

Fig. 1 Generation of hematopoietic cells from pluripotent stem cells in vitro. Embryonic stem (ES) and induced pluripotent stem (iPS) cells have been differentiated into hematopoietic cells (HCs) through mesodermal cells, ancestors of HCs, by two methods: embryoid body (EB) formation and co-culture with stromal cells in vitro. These cells are potentially applicable to regenerative medicine and drug screening by manipulating their lineage specific differentiation in vitro